Spatial eco-evolutionary feedbacks mediate coexistence in prey-predator systems

Eduardo H. Colombo[1*], Ricardo Martínez-García[2], Cristóbal López[1], Emilio Hernández-García[1]

1 IFISC (CSIC-UIB), Campus Universitat Illes Balears, 07122, Palma de Mallorca, Spain
2 Department of Ecology and Evolutionary Biology, Princeton University, Princeton NJ 08544, USA

* ecolombo@ifisc-uib.csic.es

Abstract

Eco-evolutionary frameworks can explain certain features of communities in which ecological and evolutionary processes occur over comparable timescales. In the particular case of prey-predator systems, a combination of empirical and theoretical studies have explored this possibility, showing that the evolution of prey traits, predator traits or the coevolution of both can contribute to the stability of the community, as well as to the emergence of various types of population cycles. However, these studies overlook that interactions are spatially constrained, a crucial ingredient known to foster species coexistence *per se*. Here, we investigate whether evolutionary dynamics interacts with the spatial structure of a prey-predator community in which both species show limited mobility and predators perceptual ranges are subject to natural selection. In these conditions, our results unveil an eco-evolutionary feedback between species spatial mixing and predators perceptual range: different levels of species mixing select for different perceptual ranges, which in turn reshape the spatial distribution of preys and their interaction with predators. This emergent pattern of interspecific interactions feeds back to the efficiency of the various perceptual ranges, thus selecting for new ones. Finally, since prey-predator mixing is the key factor that regulates the intensity of predation, we explore the community-level implications of such feedback and show that it controls both coexistence times and species extinction probabilities.

Author summary

Evolutionary processes occurring on temporal scales that are comparable to those of ecological change can result in reciprocal interactions between ecology and evolution termed eco-evolutionary feedbacks. Such interplay is clear in prey-predator systems, in which predation alters the distribution of resources (preys). In turn, changes in the abundance and spatial distribution of preys may lead to the evolution of new predation strategies, which may change again the properties of the prey population. Here, we investigate the interplay between limited mobility, species mixing, and finite perception in a prey-predator system. We focus on the case in which predator perceptual ranges are subject to natural selection and examine, via coexistence times and species extinction probabilities, whether the resulting eco-evolutionary dynamics mediates the stability of the community. Our results confirm the existence of such eco-evolutionary feedback and reveal its potential impact on community-level processes.

Introduction

One of the major goals of ecology is to understand the mechanisms that sustain the coexistence of antagonistic species, such as one prey and its predator or competitors for common resources. Under the traditional assumption that ecological and evolutionary changes occur on very different time scales, the connection between ecology and evolution is unidirectional, with the former driving the later. Therefore, the first attempts to explain species coexistence neglected the role of evolutionary processes and relied exclusively on ecological factors, such as species neutrality [1], frequency-dependent interactions [2], and environmental heterogeneity, either in space or in time [3–7].

More recently, however, evidences that ecological and evolutionary processes can occur at congruent time-scales have been found [8–10]. This result suggests that both processes can affect each other in some situations and establish 'eco-evolutionary feedbacks' (EEFs) that may alter the ecological dynamics and the stability of communities. Due to rapid evolution, the frequency of the genotypes and their associated phenotypes within a population changes as fast as ecological variables, like population sizes or spatial distributions, and affect their dynamics. In turn, these new ecological configurations redirect the evolutionary process [11–16].

The consequences of these EEFs at the community level have been studied mainly in single-species populations and simple two-species communities [13]. In prey-predator systems, empirical studies have shown that both prey and predator traits can evolve over ecological time scales, leading to EEFs that alter some features of the dynamics of the populations [17,18]. For instance, in a rotifer-algal system, rapid prey evolution induced by oscillatory predator abundance can drive antiphase in prey-predator cycles [14]. Theoretical investigations have also suggested that prey-predator coevolution can induce a rich set of behaviors in population abundances, including reversion in the predator-prey cycles [19]. Another family of studies has focused on the role of EEFs on the stability of the community, showing that different feedbacks influence the stability of prey-predator dynamics in different ways depending on the shape of the trade-offs between the evolving traits [13,20,21].

However, despite these insightful studies, the interplay between eco-evolutionary feedbacks and spatial dynamics, a crucial aspect that often controls species interactions, remains largely unexplored in prey-predator systems. EEFs in spatially structured populations have been studied mostly for single-species populations in which evolutionary dynamics affects the rate of dispersal, either across patches or during range expansions [13,22,23]. Here, we extend those scenarios and investigate how eco-evolutionary dynamics can modulate two-species interactions in a spatially-extended prey-predator community. To this aim, we use an individual-based model in which both species have limited mobility and predation is nonlocal, i.e., only preys within a finite region around the predator are susceptible to predation. The radius of this region defines predators perceptual range, which in our model varies across the population and is subject to natural selection. Perceptual ranges, generally defined as the maximum distance at which individuals can identify elements of the landscape, vary tremendously within species and have a strong impact on determining the success of foraging and haunting strategies via several trade-offs [24,25]. For instance, large perceptual ranges increase the number of potentially detectable preys, but may lead to a reduced attacking efficiency, as information is integrated over a large area [25–27], whilst also allows for the presence of prey crowding effects [28,29]. These trade-offs bound the evolution of the perception range, setting a finite optimal value. Overall, due to its large intraspecific variability, important contribution to individual fitness and sensitivity to species spatial distribution, the perceptual range arises as an important trait for studying the interplay between its evolutionary dynamics and spatial ecological

processes within the community.

In fact, our results reveal the existence of a feedback between the evolution of the predator perceptual range and species spatial distributions that controls community-level processes. We perform a systematic investigation of the predator-prey dynamics under different levels of mobility and mutation intensities and characterize the community long-time behavior by species mixing measures, by the distribution of predators' perceptual range and by species coexistence time period. Depending on individual mobility (and the interactions taking place), different levels of spatial mixing emerge, ranging from segregation to high mixing, and select for different perceptual ranges. Simultaneously, due to predation, perceptual ranges alter the spatial mixing of preys and predators, establishing an eco-evolutionary feedback. Importantly, since species mixing modulates the intensity of the prey-predator interaction, the eco-evolutionary feedback strongly influences the stability of the community. A diagram with the coupling between species spatial distribution, individual traits and community level processes is shown in Fig 1. Finally, although derived for the particular case of a prey-predator system, these results will more generally improve our understanding of how information gathering over nonlocal spatial scales may influence species interactions and how evolutionary processes may alter the ecological dynamics and stability of spatially-structured multispecies communities.

Results

To investigate the interplay between spatial structure and evolution of the range of nonlocal interspecific interactions in a simple community (see the diagram shown in Fig 1) we build an individual-based prey-predator model (see Methods for full details) in which individuals of both species move within a square environment of lateral length L (and periodic boundary conditions). Movement is modeled using Brownian motions with diffusion coefficients D_p for predators and D_v for preys (v stands for victims), which influences the spatial distribution of the populations (Fig 2). Large diffusion leads to homogeneously distributed populations, whereas clusters form at low diffusion due to the existence of reproductive pair correlations [30].

We implement a stochastic population dynamics in which prey reproduction and predator death occur with constant rates r and d, respectively. The predation rate, c, however, is dictated by the availability of preys and the efficiency of the predator to attack them. Mathematically, this can be written as $c(R) = E(R)M_v(R)$, where $M_v(R)$ accounts for the number of preys within predator's perceptual range, R, and $E(R)$ is the attacking efficiency up to distance R. We have defined the perceptual range R, different for each predator, as the maximum distance measured from the position of the predator at which a prey can be detected. Note that $0 \leq R \leq L/2$, due to the periodic boundary conditions. If the perception range is large, the number of available preys increases, but it does so at the cost of a reduced predation likelihood. We implement this trade-off through the attacking efficiency $E(R)$, which we assume to be a decreasing function of the predation range. The particular shape of $E(R)$ may depend on several factors, related to prey, predator behavior or environmental features. To be specific, we assume that the attacking efficiency decays exponentially with the perception range as $E(R) = c_0 \exp(-R/R_c)$, where c_0 is a maximal efficiency and R_c fixes how quickly this efficiency decays as the perception range increases. For this particular choice, and considering a homogeneous distribution of preys, $M_v(R) \propto \pi R^2$, the predation rate $c(R) \propto R^2 \exp(-R/R_c)$ is thus maximized for $R_h^\star \equiv 2R_c$. We will use this value $R_h^\star$ as a reference to measure the effect of mutations and nonhomogeneous distributions of individuals on the optimal perception range.

The trade-off between perception and attacking efficiency, as well as the choice of E

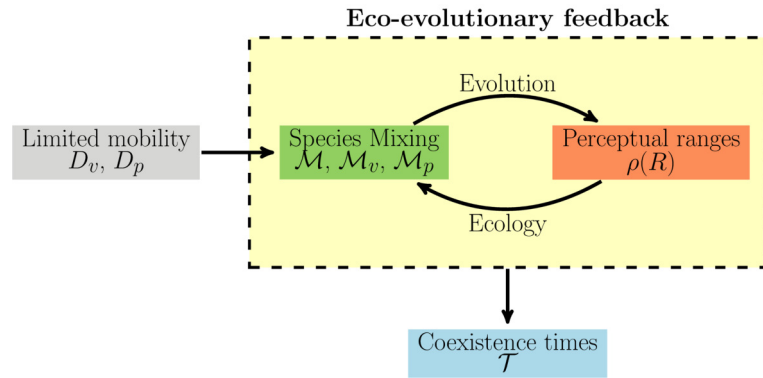**Fig 1. Schematic representation of the eco-evolutionary framework.** In the gray box the microscopic parameters D_v and D_p are the prey and predator diffusion coefficients that set the level of mobility. The rest of the elements are properties at the community level that arise from them and from the demographic rates. In the green box species spatial distribution characterization though the mixing measures $\mathcal{M}, \mathcal{M}_p, \mathcal{M}_v$. In the orange box predators perceptual range distribution $\rho(R)$. In the blue box, community coexistence times $\mathcal{T}$. Arrows indicate the influence between the elements through different processes.

such that predation rate maximizes at intermediate scales of perception, is grounded on previous theoretical studies showing that foraging success decreases when individuals have to integrate information over very large spatial scales [25–27, 31]. Another example that can illustrate the trade-off between perception and predation efficiency is that of flying predators, whose flight altitude influences the area where preys can be detected. However, even though flying at high altitudes opens the field of view and possibly the number and frequency of prey detection it may also have a negative effect on predation success, since attacks are initiated from further away. Note that we do not model the attack process, that we consider to be instantaneous. Thus, the predator mobility described by the diffusion coefficient D_p refers to the predator motion while searching.

Ultimately, prey consumption will support predator reproduction. To model this, whenever a prey is caught by a predator, there is a probability b for the predator to reproduce. Hence, predators reproduction rates are determined by the interplay between their perception range and the spatial configuration of preys. Ignoring any complex phenotype-genotype relationship and the role of the environment [32], we assume that newborns inherit the perceptual range from their parent, with some possible mutation that adds to R a random perturbation sampled from a Gaussian of zero mean and variance σ_μ^2. This trait remains unchanged during predators' lifetime. The mutation intensity σ_μ sets the speed of the evolutionary process. Mathematical details of the model and its implementation are provided in Methods.

Since we are interested in how the coupling between limited dispersal and evolution in the perception ranges influences the stability of the community, we fix all the model parameters (see Methods) except the intensity of the mutations in R, σ_μ, and the diffusion coefficients D_v and D_p, which are the control parameters that drive the degree of mixing in the population (for computational convenience, different values of L will also be used). Therefore, for a given pair of diffusion rates and a mutation intensity, three linked community-level features emerge: the species spatial distributions, the distribution of predator perceptual ranges (i.e., the outcome of the evolutionary dynamics) and the coexistence time of the populations. In the following sections we
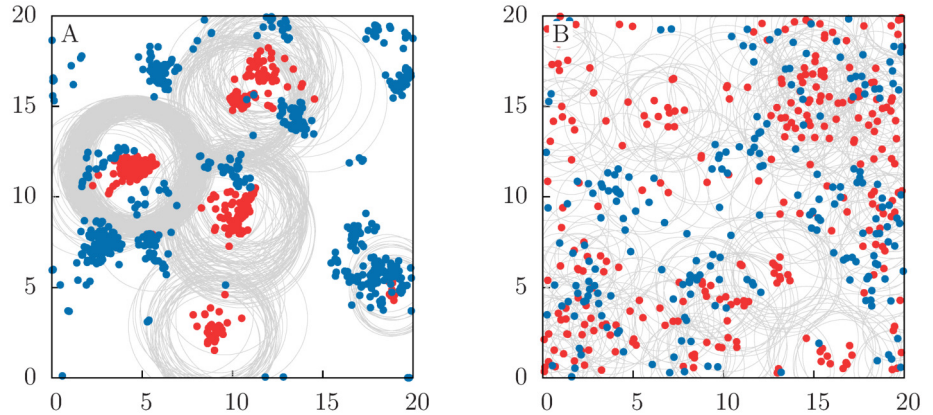
Fig 2. Species spatial distribution. Spatial distribution of predators (red) and preys (blue) in the long-time regime for (A) low and (B) high mobility, with $D_p = D_v = 0.1$ and $D_p = D_v = 1$, respectively. Gray circles indicate the perception area of the predators, which is subject to evolutionary dynamics (with $\sigma_\mu = 0.1$, see Methods for details). The habitat is a square domain with size $L = 20$ and periodic boundary conditions. See S1 Movie and S2 Movie to visualize the model dynamics.

examine each of these features more in depth. 132

Species spatial distributions 133

For fixed prey birth and predator death rates, the spatial distribution of preys and 134
predators is determined by three characteristic spatial scales, controlled by D_v, D_p and 135
R. Fig 2 shows that for large diffusivities (right panel) both predators and preys are 136
homogeneously distributed, whereas they form clusters for low diffusion coefficients (left 137
panel). 138

In order to quantify population clustering within each species, as well as interspecies 139
mixing, we define the indicators $\mathcal{M}_v$ and $\mathcal{M}_p$ for the former and $\mathcal{M}$ for the latter. 140
These quantities are defined in terms of the Shannon index or entropy [33–35], 141
conveniently modified to correct for the effect of fluctuations in the number of 142
individuals (see Methods for the mathematical definitions). The interspecies mixing $\mathcal{M}$ 143
takes values between 0 and 1, with 0 indicating strong species segregation and 1 144
representing the well-mixed limit. On the other hand, $\mathcal{M}_p$ and $\mathcal{M}_v$ also take values 145
within the same range, but since these metrics focus on one single species, $\mathcal{M}_\alpha = 0$ 146
indicates a high level of clumping of species α ($= v$ or p) and $\mathcal{M}_\alpha = 1$ a uniform 147
distribution of the corresponding species. 148

The mixing measures are sensitive to the diffusion coefficients and predators 149
perception range. First, we analyze the spatial distribution of species at a fixed 150
mutation intensity and in the long-time limit, i.e., once the distribution of perceptual 151
ranges reached a stationary form. 152

For a fixed mutation-noise standard deviation ($\sigma_\mu = 0.1$), Fig 3 shows the average 153
values of the mixing measures in the long-time regime as a function of the individuals 154
mobility, revealing a complex interaction between mobility and species mixing. When 155
both preys and predators have the same diffusion coefficients, $D_v = D_p$, all the mixing 156
indices increase with mobility (Fig 3A). However, when species have different diffusion 157
coefficients, $D_v \neq D_p$, the mixing may become a non-monotonic function of one of the 158

diffusion coefficients. For the particular case shown in Fig 3B, the prey mixing still increases monotonically with D_v, but the interspecies and the predator mixing show a maximum at intermediate D_v. Prey population can be seen as a dynamical resource landscape that drives the spatial distribution of predators. Increasing D_v always leads to a more uniform distribution of preys. However, the extent to which this also leads to more uniform distributions of predators is limited by D_p (which in Fig 3B is fixed at a low value $D_p = 0.1$). In particular when $D_v \gg D_p$ predators cannot follow the dynamics of the preys and both $\mathcal{M}$ and $\mathcal{M}_p$ decrease with increasing D_v.
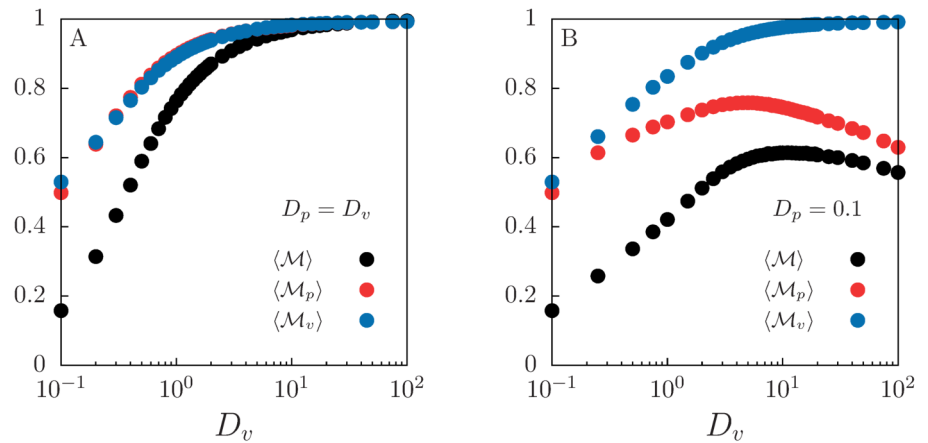

Fig 3. Species mixing. Average predator-prey mixing $\langle \mathcal{M} \rangle$ and prey and predator mixing, $\langle \mathcal{M}_v \rangle$, $\langle \mathcal{M}_p \rangle$, respectively, for different individuals mobility with (A) $D_p = D_v$ and (B) $D_p = 0.1$. Mutation intensity is $\sigma_\mu = 0.1$ and habitat size $L = 10$. Average is performed over time and 10^4 realizations in the long-time regime.

Next, we explore the effect of the mutation intensity on the long-time average interspecies mixing, $\langle \mathcal{M} \rangle$ (angle brackets indicate average over time and realizations). In the non-evolving case, i.e. in the no-mutation limit ($\sigma_\mu = 0$) and setting the same perceptual range R for all predators, mixing is a convex function of R, showing a minimum for intermediate perception ranges (see S1 Fig). The values of R giving minimum mixing without evolution (S1 Fig) are close to the ones dynamically achieved under evolution (see section Evolutionary dynamics), stressing the fact that predation reduce interspecies mixing. When mutations are allowed ($\sigma_\mu > 0$), however, predators' perceptual range are not free parameters, but an outcome of the eco-evolutionary dynamics and thus controlled by the individuals mobility and mutation intensity. In particular, in Fig 4, fixing $D_v = D_p$, we show how σ_μ changes the predator-prey mixing curve shown in Fig 3A. To this aim we define the relative change with respect to the no-mutation limit case ($\sigma_\mu = 0$), in which all predators have the optimal perceptual range $R^\star$ (see section Evolutionary dynamics),

$$\Delta \langle \mathcal{M} \rangle (D_v, D_p | \sigma_\mu) \equiv \frac{\langle \mathcal{M} \rangle (D_v, D_p | \sigma_\mu) - \langle \mathcal{M} \rangle (D_v, D_p | \sigma_\mu = 0)}{\langle \mathcal{M} \rangle (D_v, D_p | \sigma_\mu = 0)}, \qquad (1)$$

where brackets indicate average over time and realizations in the long-time regime.

While at low mobility interspecies mixing is reduced as mutation noise σ_μ increases (i.e. more segregated predator-prey distributions will be obtained for larger mutation intensity), at high mobility the effect is the opposite. Particularly, at intermediate mobility, the mixing suffers a maximum positive change. These effects arise mainly from
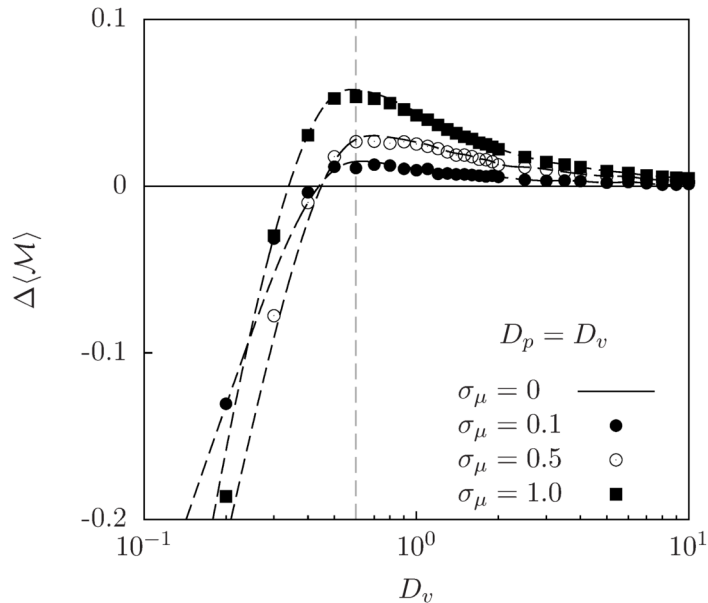
Fig 4. Mixing dependency on mutation intensity. Average predator-prey mixing change relative to the no-mutation case, $\Delta\langle\mathcal{M}\rangle$ defined in Eq (1), as a function of the diffusion coefficients $D_v = D_p$ and for different levels of mutation noise variance. Habitat size $L = 10$. Symbols indicate the results from simulations. Dashed lines are smooth fits to simulation data for different mutation intensities. The horizontal continuous line $\Delta\langle\mathcal{M}\rangle = 0$ is the no-mutation case ($\sigma_\mu = 0$). Vertical line indicates the maximum mixing for $\sigma_\mu = 1.0$.

the mutation-induced variability in the values of R in the predator population, which will be discussed in the next section.

Evolutionary dynamics

In our model we assume that predators perceptual range (and thus predator reproduction rates) are subject to natural selection. We neglect any complexity in the genotype-phenotype relationship and the role of environment [32], assuming that the value of the trait R of a predator is passed to its offspring, with some variation due to mutation, remaining unchanged during its lifetime. Natural selection is at work since, depending on the spatial distribution of preys, some perceptual ranges are favored against the others and hence tend to be overrepresented within the populations.

Homogeneous limit. In the $D_v, D_p \to \infty$ limit (which leads to $\mathcal{M}, \mathcal{M}_v, \mathcal{M}_p \to 1$), the populations of preys and predators are randomly distributed in space and well-mixed with each other. In this homogeneous mean-field limit, it is possible to derive an equation for the dynamics of the distribution of perceptual ranges in the population, $\rho(R)$. We define its normalization such that its integral gives, at each time, the total number of predators, N_p: $\int dR\rho(R) = N_p$. On average, and in the absence of any mutation effect, the encounters between preys and predators lead to an expected rate of change of $\rho(R)$, $\widetilde{\rho(R)}$, given by

$$\widetilde{\rho(R)} = b\rho(R)\langle c(R)\rangle_p, \tag{2}$$

which is proportional to the mean predation rate $\langle c(R)\rangle_p$ (averaged over all predators

that experience different environments but with the same R) multiplied by the probability b of birth after a predation event. In this homogeneous limit, and if the number of individuals is large enough so that we can neglect demographic fluctuations, the expected number of preys within a radius R is $\langle M_v(R)\rangle_p = \pi R^2 v$. v is the (uniform) density of preys. Thus $\langle c(R)\rangle_p = \langle E(R)M_v(R)\rangle_p = c_0\pi R^2 v e^{-R/R_c}$ (see Methods for further details). Next, considering the effect of mutations, which changes the perception ranges of the new individuals, and adding the contribution from the predator death at fixed rate d, the distribution of perception ranges evolves according to

$$
\begin{aligned}
\frac{\partial \rho(R,t)}{\partial t} &= \int_0^{L/2} G_\mu(R,R')\widetilde{\rho(R')}dR' - d\rho(R) \\
&= \pi b c_0 v \int_0^{L/2} G_\mu(R,R')\rho(R')(R')^2 e^{-R'/R_c}dR' - d\rho(R) ,
\end{aligned}
\tag{3}
$$

while prey-density changes follow

$$
\begin{aligned}
\frac{dv}{dt} &= rv - \int_0^{L/2} \langle c(R)\rangle_p \rho(R)dR , \\
&= rv - \pi c_0 v \int_0^{L/2} R^2 e^{-R/R_c}\rho(R)dR ,
\end{aligned}
\tag{4}
$$

where the first term represents prey birth at constant rate r and the second one accounts for predation.

The integral kernel G_μ relates newborn with parental perceptual ranges and thus depends on mutations. Recall that these mutations are random perturbations that follow a Gaussian distribution of zero mean and variance σ_μ. The kernel G_μ should also account for boundary conditions in R, such that mutations leading to perception ranges that would be negative or larger than half of the system size are rejected. Thus, G_μ is a Gaussian function restricted to the interval $[0,L/2]$,

$$
G_\mu(R,R') = \begin{cases} \frac{1}{\mathcal{N}(R)}e^{\frac{-(R-R')^2}{2\sigma_\mu^2}} & 0 < R' < L/2 \\ 0 & \text{else} \end{cases} ,
\tag{5}
$$

where $\mathcal{N}$ is a normalization factor given by $\mathcal{N}(R) = \sqrt{\frac{\pi}{2}}\sigma_\mu\left[\mathrm{erf}\left(\frac{R}{\sqrt{2}\sigma_\mu}\right) - \mathrm{erf}\left(\frac{R-L/2}{\sqrt{2}\sigma_\mu}\right)\right]$. The agreement between the theoretical prediction for the well-mixed case ($D_v, D_p \to \infty$), computed from Eqs (3)-(5), and direct simulations of the individual-based dynamics is shown in Fig 5. The infinite-diffusion homogeneous limit is implemented in the simulation by randomly redistributing predators and preys in space at each time step. Starting from any initial distribution, the maximum of the time-dependent distribution $\rho(R)$, that defines the dominant perceptual range $R^\star$, approaches values near the one that gives the maximum catching rate $R_h^\star = 2R_c$ (Fig 5A). The long-time dominant value corresponds exactly to the optimal one, $R_h^\star$, when mutation is negligible. As mutation intensity σ_μ increases, the long-time distribution $\rho(R)$ becomes wider and there is also a small shift towards larger values (Fig 5B), which arises due to the asymmetric form of the catching rate $\langle c(R)\rangle_p$. Thus, the dominant R has a main component set by the optimal value and a small positive shift due to mutation effects. These changes, specially the strong effect observed in the perceptual range variability, are the ones responsible for the feedback in the predator-prey mixing shown in Fig 4. The corresponding result from individual-based simulations is obtained by averaging over independent runs the perceptual range distribution $\rho(R)$ at each time, and extracting its maximum $R^\star$ at that time. The agreement between both results persists as long as the number of individuals

is large. Lastly, note that Eqs (3)-(4), recover the classical Lotka-Volterra predator-prey equations in the limit of vanishing trait variability, $\rho(R,t) \to N_p \delta(R - R^\star)$.
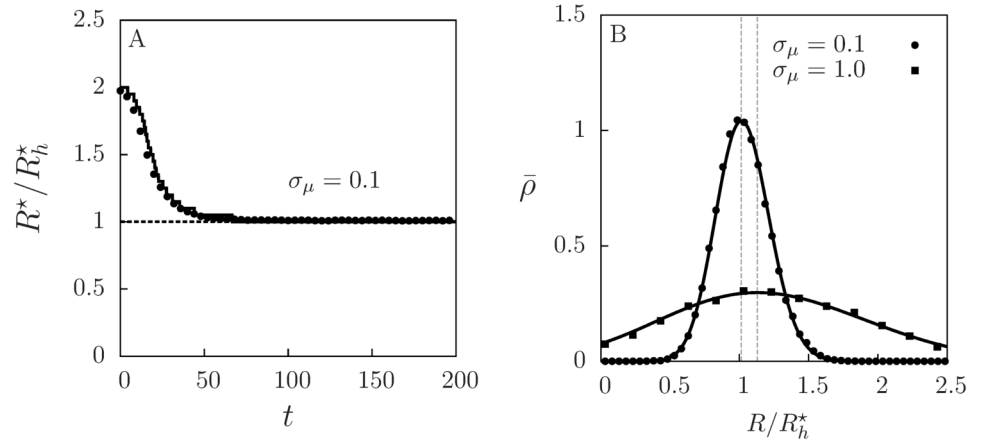

Fig 5. Evolutionary dynamics in the homogeneous limit. (A) Temporal evolution of the dominant perception range R^* (the mode, i.e. the maximum of $\rho(R)$), relative to the one giving the maximum predator growth in the homogeneous case, R_h^*, for $\sigma_\mu = 0.1$ and a system size $L = 40$. Solid line is obtained from numerical solution of Eqs (3)-(4), and dots give the maximum of the distribution $\rho(R)$ obtained from the average of 100 independent runs of the individual-based model with $D_v, D_p \to \infty$. In all cases the initial distribution gives weight only to $R = 2R_h^*$. (B) Probability density for finding a perception range value R in the population of predators, $\bar{\rho}(R) = \rho(R)/N_p$, in the long-time regime, for low and high mutation noises. Dots correspond to simulations of the individual-based model (with $D_v, D_p \to \infty$, average over 100 runs) and solid lines to the numerical solution of Eqs (3)-(4). Dashed vertical lines show the position of the mode of each distribution.

Finite mixing case. For the general case of limited dispersal, far from the well-mixed scenario, some of the features shown in Fig 5 still persist, but modified due to the underlying spatial distribution of preys and predators. Since the analytical approximations derived for the infinite diffusion limit are not valid, we study this scenario via numerical simulations of the individual-based model. In Fig 6A we show that, starting from different initial distributions of R, the location R^* of the maximum of the average distribution $\rho(R)$, giving the most probable value of R, evolves in time towards a value that depends on the mobility of both species, with reduced mobility favoring larger perceptual ranges (Fig 6B). The change in $\rho(R)$, both with time and with species mobility in the long-time limit, is shown in S2 Fig. The most probable perception range decreases with increasing predator and prey diffusion rates, and it approaches the homogeneous value as a power-law (see inset of Fig 6B).

We identify that the change in the dominant perception range due to mobility is well captured by the prey mixing parameter $\mathcal{M}_v$: Fig 6C shows the dominant R in the long-time regime as a function of prey clumping. We extract that

$$\frac{|R^\star - R_h^\star|}{R_h^\star} = (1 - \langle \mathcal{M}_v \rangle)^\gamma , \qquad (6)$$

with $\gamma \simeq 1.5$ ($\gamma \simeq 0.5$) when fixing $D_p = D_v$ ($D_p = 0.1$) and mutation intensity $\sigma_\mu = 0.1$. This relation is valid for low mutation intensity, such that in the well-mixed
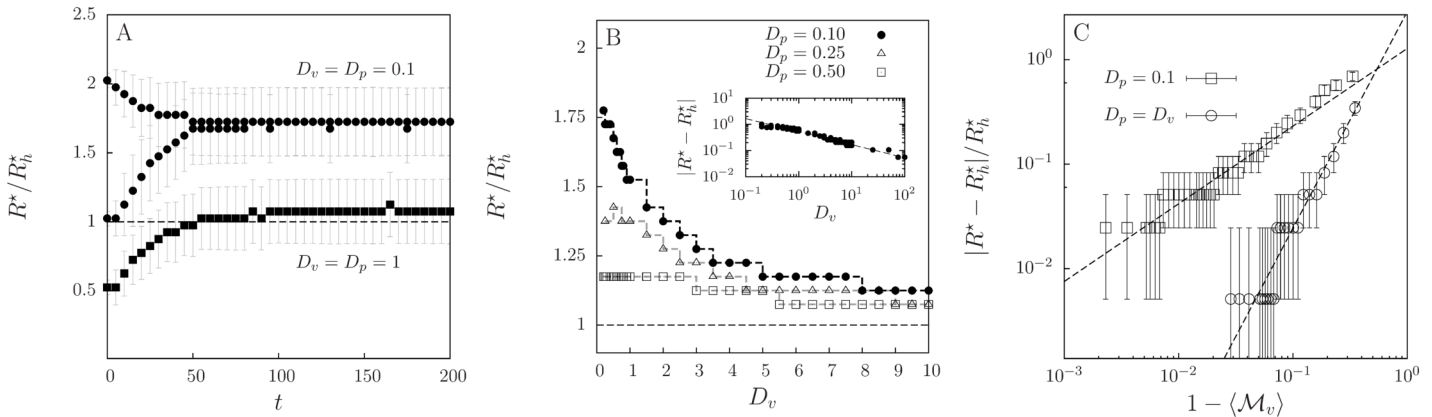
Fig 6. Dominant perceptual range: from the segregated to the well-mixed scenario. (A) Temporal evolution of the location $R^\star$ of the maximum in the average perception range distribution $\rho(R)$ (average over 10^4 runs), relative to the optimal perception range for homogeneous populations, $R_h^\star$, for high ($D_v = D_p = 1.0$) and low ($D_v = D_p = 0.1$) diffusion coefficients. Two different sharply-localized initial population distributions are used in each case. Bars indicate the standard deviation of $\rho(R)$ around $R^\star$. (B) Dominant perception range relative to the homogeneous-case optimal, $R^\star/R_h^\star$, as a function of prey and predator diffusion rates. Dashed lines are guides to the eye and indicate the discretization $\Delta R = 0.1$ used for the numerically obtained $\bar{\rho}$. Inset shows the asymptotic approach of $R^\star$ to the homogeneous optimal, $R_h^\star$, as D_v increases with $D_p = 0.1$. (C) The relative difference between the dominant range in the simulations and the optimal one in the homogeneous case, $|R^\star - R_h^\star|/R_h^\star$ versus $1 - \langle \mathcal{M}_v \rangle$, which measures prey clumping (averaged over time and realizations in the long-time regime), for different values of prey diffusion D_v, while keeping $D_p = D_v$ (circles) or $D_p = 0.1$ (squares). Bars indicate bin size of the computationally obtained $\rho(R)$. Dashed lines represent the power-law expressions set in Eq. (6), with $\gamma \simeq 1.5$ for $D_p = D_v$ and $\gamma \simeq 0.5$ for $D_p = 0.1$. Habitat lateral length $L = 10$ and mutation intensity $\sigma_\mu = 0.1$ in all the panels.

scenario, $\mathcal{M}_v \to 1$ (achieved for large diffusivities), we have $R^\star \simeq R_h^\star$. The prey mixing is the main quantity that controls the dominant perceptual range as it condense the spatial information of the environment experienced by predators. As prey form clusters, $\mathcal{M}_v < 1$, predators typically find preys at distances larger than in the homogeneous case (see Fig 2). So, in the low-mobility regime their predation rate only becomes significant for larger R.

Coexistence times and extinction probabilities

We have observed in the previous sections that the eco-evolutionary feedback between evolution of perception ranges and species mixing controls predation rates. Thus, we expect it to impact also the population dynamics and the stability of the community. To quantify this, we measure the coexistence time between preys and predators, $\mathcal{T}$, and the probability that preys get extinct before the predators, β, as a function of the predator and prey mobilities and the intensity of the mutations. Mean coexistence time $\mathcal{T}$ is defined as the time until either preys or predators get extinct, averaged over independent model realizations, and β is obtained as the fraction of realizations in which predators persist longer than preys. Since preys are the only resource for

predators, these will shortly get extinct following prey extinctions. On the contrary, when predator extinctions occur first, preys grow without constraint because we do not account for interspecific competition. For each realization we use initial conditions that lead to a very short transient after which spatial structure and the perceptual range distribution achieve its long-time behavior. In most cases, the well-mixed mixed scenario with uniformly distributed perceptual range allow this to happen. Nevertheless, for small mutation rates ($\sigma_\mu < 0.1$), the evolutionary time scales become comparable to the coexistence times and in these cases we need to fast forward the evolutionary component of the transient dynamics by setting an initial condition for the perceptual range distribution close to the expected at long times.

In Fig 7A we show the mean coexistence time $\mathcal{T}$ as a function of predator and prey diffusion coefficients, assuming $D_v = D_p$, for different mutation intensities. This curve is a complex outcome of the values of the dominant perceptual range, the associated catching rate, and the degree of mixing that arise from limited dispersal. Long coexistence would occur when there is a balanced mixing between preys and predators, which allows predation in a controlled manner, preserving prey population. For small mutation intensity, the coexistence time, which is maximum at low diffusivities, decreases as the diffusion coefficients increase until reaching a minimum at intermediate mobility. Then, $\mathcal{T}$ increases slowly, approaching asymptotically the well-mixed case. As mutation increases there is a clear change in the depependence of $\mathcal{T}$ with the diffusivities. The maximum of $\mathcal{T}$ is shifted to intermediate values of diffusivities. This is one of the relevant results of this paper. This result comes from the effect that mutation intensity (when non-negligible) has in predator-prey mixing, as shown in Fig 4: mixing decreases for low mobility and increases at intermediate values of the mobility. Since mixing controls interspecies interaction, a key ingredient for coexistence, this is translated to the behavior of $\mathcal{T}$. As seen in Fig 7A, the level of mobility at which the increase in mixing is maximum (vertical dashed line, from Fig 4) roughly matches the location of the maximum $\mathcal{T}$.

As discussed in the previous sections, mutation intensity interferes in predator-prey mixing mainly through its influence in perceptual range variability (see Fig 5B), establishing the feedback that mediates community coexistence. Despite that, variability in R brings secondary effects. For instance, variability gives resilience to the community, since it allows predators to overcome time periods in which, due to fluctuations in the spatial distribution of preys, the (on average) optimal R is temporarily suboptimal. Also, variability reduces overall predators' predation success.

Finally, we calculate the probability that preys become extinct before predators β, as a function of D_v (which is taken to be equal to D_p) for different values of σ_μ (Fig 7B). Even though the most likely event is that predators disappear before preys ($\beta < 0.5$), as the diffusion coefficients increase from very small values, we observe an increase on β passing through a maximum at intermediate values of diffusivities. Despite the nonlinear effects between catching rate and species spatial distributions, β generally becomes large as mixing increases (see Fig 3A and Fig 7B), since it enhances predation. Note that, comparing Figs 7A and 7B, the maximum β (high predation) is not related to maximum coexistence, which calls for an ideal balance between catching and prey population preservation. The influence of mutation intensity in the profiles shown in Fig. 7B, again, is due to the feedback in the interspecies mixing shown in Fig 1, which regulates the level of predation. Hence, prey extinction is reduced at low mobility but increased at high mobility, shifting the profile.
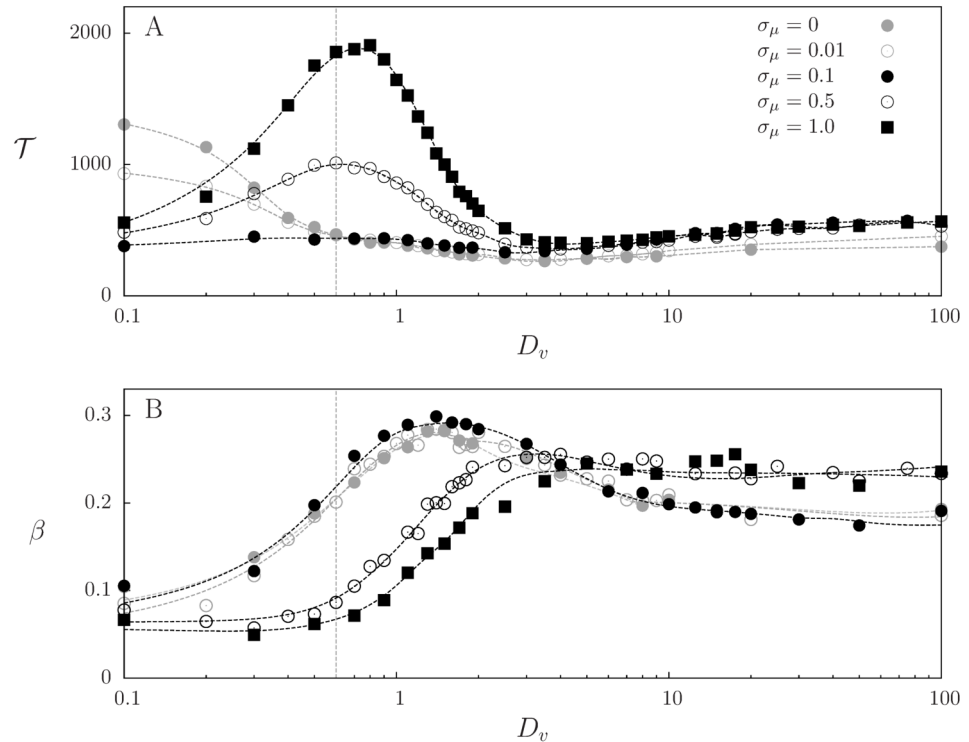
Fig 7. Community coexistence times and prey extinction probability. (A) Mean coexistence time $\mathcal{T}$ and (B) Probability of prey extinction before predators, β, as function of the diffusion coefficients $D_p = D_v$ for different levels of mutation noise intensities with system size $L = 10$. Initial conditions are preys and predator uniformly distributed in space with uniformly distributed perception range R, and results were extracted from 5×10^3 realizations. Dashed lines are smooth fits to guide the eyes. Vertical dashed lines indicate the diffusivity value at which the increase of mixing with respect the no-mutation case is maximum (from Fig 4, $\sigma_\mu = 1.0$)

Summary and Discussion

Using an individual-based model, we have investigated whether the evolutionary dynamics of predator perceptual ranges influences the stability of spatially-structured prey-predator communities. First, we studied how different levels of interspecies mixing arise due to limited mobility and variability in the perceptual range induced by the intensity of mutations. Second, we evaluated the consequences of the interplay between species mixing and the predator perception range in other community-level outcomes. Our results reveal the existence of an eco-evolutionary feedback between interspecies mixing and predators perception: species mixing selects a certain distribution of perceptual ranges due to an underlying perception-vs-attacking efficiency trade-off; in turn, the distribution of perceptual ranges reshapes species spatial distribution due to predation. More specifically, when species mobilities are low, preys and predators form monospecific clusters and thus segregate from each other. Therefore, preys often inhabit regions of the environment that are not visited by predators, which forces the evolution of larger predatory perception. Conversely, as mobility becomes higher, species mixing increases and short-range predation is favored. Finally, our results indicate that

community stability and diversity, characterized by the mean coexistence time and prey extinction probability, are strongly controlled by the eco-evolutionary feedback. In particular, the average coexistence time is maximum when the interaction between species mixing and predator perception ranges yields in predation rate that is large enough to sustain the population of predators but low enough to avoid fast extinctions of preys.

The two community-level metrics, mean coexistence time and species extinction probabilities, provide important information about the diversity of the community at different scales [36]. From a metapopulation perspective, each model realization performed to obtain these observables can be related to the dynamics taking place within distinct local regions, known as patches. In our case, since realizations are independent, these patches are isolated (not coupled by dispersal events) and constitute a "non-equilibrium metapopulation" [37]. In this context, the mean coexistence time is a proxy for alpha (intra-patch) diversity, i.e. how long species coexist in each patch, whereas species extinction probabilities inform about the beta (inter-patch) diversity, i.e., how many patches are expected to be occupied by preys and how many by predators once one of the species has been eliminated. Using a mathematical reasoning, the fraction of patches in which predators and preys coexist at any time t is given by $P(t) = \int_t^\infty p(t')dt' = 1 - \int_0^t p(t')dt'$, where $p(t)$ is the distribution of coexistence times. Supported by our numerical simulations, we can approximate $p(t) \simeq \mathcal{T}^{-1}e^{-t/\mathcal{T}}$ (except for coexistence times that are much smaller than the mean, see S3 Fig). Therefore, $P(t) \simeq 1 - e^{-t/\mathcal{T}}$. The fraction of patches occupied only by preys is given by $(1-\beta)(1-P(t))$, and the fraction of patches in which overexploitation has caused prey extinction is given by $\beta(1-P(t))$. Hence, the mean coexistence time $\mathcal{T}$ and the prey extinction probability β quantify the diversity of the community at different spatiotemporal scales [33, 36, 38], that might serve as important guides for the design of ecosystem management protocols [38, 39].

Since we were interested in studying whether the spatial coupling between mobility and perception could lead to an eco-evolutionary feedback when both processes occur at comparable time scales [14, 15], we kept all the characteristic time scales of the system fixed, except those related to diffusion and the evolutionary dynamics of perceptual ranges. In this scenario, provided that evolution is fast enough, the spatial distribution and the distribution of perceptual ranges relax to their stationary values in timescales much shorter than the characteristic time scales at which community-level processes occur, defined by the mean coexistence time. Under this condition, the long-time regime is well-defined and can be characterized by constant quantities. A sensitivity analysis on reproduction rates and initial conditions reveals that, as far as this relationship between time scales is maintained, both the existence of the eco-evolutionary feedback and its impact on community stability and diversity remain unaffected. This condition can be broken, for instance, if predator and prey birth-death rates are small, or too unbalanced, producing very short coexistence times. Our results are also robust against changes in the source of individual-level trait variability, as individual-level trait variability affect mixing in a similar way. In this work, we have considered the case in which variability is induced by mutation in the transmission of the trait, but variability can be rooted in non-inheritable properties, such as body size or the individual internal state (level of hunger, attention...) [25], that do not introduce spatial correlations between trait values. We have seen that sampling predators' newborn perceptual range from a suitable fixed distribution (being independent on the parents' trait), we are able to mimic the results shown in Fig. 7. This implies that different processes that promote variability can control community coexistence.

Finally, although we have focused here on a prey-predator dynamics, our results will more generally illuminate whether and to which extent the interplay between species
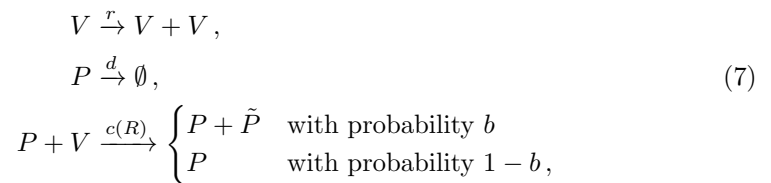
spatial distributions and evolution shaping the range of ecological interactions and information gathering processing may determine several community-level outcomes, such as diversity, stability and the distribution of traits. Therefore, our study opens a broad range of questions and directions for future research. First, we have limited to the case in which only predator traits can evolve, whereas evolution of prey traits has been also shown to impact profoundly the population dynamics of both species in well-mixed settings [21]. A natural extension of our study would be to explore such scenario in a spatially-extended framework as the one introduced here. More complex possibilities, such as the co-evolution of traits in both species could also shed some light on the possible existence of new population dynamics [19] or more general evolutionary processes, such as arm races in phenotype space (red queen-like dynamics) instead of trait distributions reaching a stationary configuration [40]. Different movement models, such as Lévy flights instead of Brownian motion, can modify both the optimal range of the interactions [27] and the emergence of clusters of interacting individuals [41], possibly leading to new community-level results. The existence of environmental features that could also affect the degree of mixing and its coupling with the range of interactions, such as the presence of external flows, would extend our results to a wider range of ecosystems in which the importance of rapid evolutionary processes has been already reported [42, 43].

Methods

Model details

The model mimics the eco-evolutionary dynamics of a prey-predator system in a square environment of lateral length L. Each predator and prey has a position in space. In addition, each predator has a different perceptual range R that determines the distribution, in the population of N_p predators, of this trait ($\rho(R)$, with $\int dR \rho(R) = N_p$). Three ingredients conform the dynamics of this individual-based model: population dynamics, evolution with mutation, and individual dispersal.

1. *Population dynamics.* The number of preys, N_v, and predators, N_p, change in time due to prey reproduction, predator death and predation. These processes are modeled as Poisson processes that occur at rates that may depend on the different densities and perceptual ranges. Each predator may die at a constant rate d and may catch a prey with rate $c(R)$ that depends on its perceptual range. If a certain predator catches a prey, it reproduces with probability b, generating at its position a new individual which inherits its trait R, possibly modified by a mutation. Preys, on the other hand, reproduce with constant rate r and die as a consequence of predation events. These processes can be written in the form of a set of biological reactions for preys V and predators P

$$
\begin{aligned}
V &\xrightarrow{r} V + V\,, \\
P &\xrightarrow{d} \emptyset\,, \\
P + V &\xrightarrow{c(R)} \begin{cases} P + \tilde{P} & \text{with probability } b \\ P & \text{with probability } 1 - b\,, \end{cases}
\end{aligned}
\tag{7}
$$

where we added the notation $\tilde{P}$ to indicate that the predator newborn might have its trait slightly modified from the parental value due to mutation (see Eq (10) below).

Each predator detects preys within a disk of radius given by its perceptual range R, with every prey inside that region equally likely to be caught. Following

previous results that link the perceptual ranges, information gathering and foraging success [25–27, 31], the model accounts for a trade-off between perceptual range and predation efficiency $E(R)$, such that while large perceptual range increases the potential number of preys, predation efficiency decreases. Combining these effects, for a given predator the predation rate can be written as

$$c(R) = E(R)M_v(R), \tag{8}$$

where $M_v(R)$ is the number of preys within the predation disk of radius R centered at the position of each predator. Since $M_v(R)$ is a monotonically growing function of R, the shape of E determines whether the predation rate maximizes at a certain perceptual range. The efficiency function E is expected to introduce an upper bound to viable perceptual ranges. This conditions is fulfilled if, for large R, the efficiency decays faster than the increasing number of preys in the range, $M_v(R)$. In the case of homogeneously distributed particles, $M_v(R) \propto R^2$. In this case, the catching rate c has a nontrivial maximum at a finite value of R if E decays faster than R^{-2}. To be specific, an exponential decay is assumed for the attacking efficiency,

$$E(R) = c_0 e^{-R/R_c}, \tag{9}$$

where R_c sets the distance at which E significantly decays and c_0 is proportional factor. For the spatially homogeneous case, we find that $c(R) \propto R^2 \exp(-R/R_c)$, which has a maximum at $R_h^\star \equiv 2R_c$. This optimal value $R_h^\star$ is used as a reference in our results.

2. *Evolution with mutation.* Each predation event is followed by the possible reproduction of the predator, occurring with probability b. In this case, besides inheriting the parental position, the newborn individual also inherits the parental perceptual range, R, but with an added random perturbation, ξ_μ, which models mutations and thus giving rise to a modified value of the trait $\tilde{R}$,

$$\tilde{R} = R + \xi_\mu. \tag{10}$$

ξ_μ is a zero-mean Gaussian variable whose variance, σ_μ^2, regulates the intensity of the mutations. In order to avoid perceptual ranges that exceed system size or are negative, mutations leading to $R < 0$ or $R > L/2$ are rejected. We neglect any complexity in the genotype-phenotype map, so that we consider the phenotypic trait R to be directly determined by the parental one and the mutations.

3. *Individual dispersal.* Individuals are assumed to follow independent two-dimensional Brownian motions with diffusion constants D_v and D_p for preys and predators respectively. The position of every individual is updated after each time step Δt (to be defined by the Gillespie algorithm described below) by sampling a turning angle, θ, and a displacement, ℓ. The turning angle follows a uniform distribution between $[0, 2\pi)$, and the traveled distance is obtained from the absolute value of a normal random variable with zero mean and variance proportional to the individual's diffusion coefficients. Periodic boundary conditions are implemented. Mathematically, this position updating for individual i can be written as

$$\mathbf{x}_i \to \mathbf{x}_i + \ell\hat{\theta} \quad \forall i \in \{1, 2, \ldots, N_p + N_v\}, \tag{11}$$

where $\hat{\theta}$ is a random direction and ℓ the length of the displacement of the jump, sampled from $p(\ell > 0) \propto \exp[-\ell^2/(2\bar{\ell}^2)]$, being $\bar{\ell} = \sqrt{2D_i\Delta t}$ with $D_i = D_v, D_p$ the individual's diffusion coefficient and Δt the simulation time step as will be detailed below.

Model implementation: the Gillespie algorithm

We implement the stochastic birth-death dynamics, occurring at Poisson times depending on the respective rates, following the Gillespie algorithm [44–46]: First, from a configuration with N_p predators and N_v preys, the predation rate $c(R_i)$ is computed for each predator, of perceptual range R_i. Next, recalling that predator death (d) and prey reproduction (r) rates are the same for all individuals, the total event rate is computed [44] as $g = rN_v + \sum_{i=1}^{N_p}[c(R_i) + d]$. Then, we compute the time-step Δt to the next demographic event as $\Delta t = \zeta\tau$ where ζ is an exponentially distributed random variable with unit mean and $\tau \equiv 1/g$, the average time to the next event. After this Δt, a single event will occur, prey reproduction, predation or predator death, chosen from all the possible events (and individual involved) with probability proportional to the contribution of the respective rate (see Eq (7) and (8)) to the total rate g. If predator death or prey reproduction occur, we simply remove or generate a new individual at parents' position, respectively. If predation occurs, a prey randomly chosen within the perception range of the selected predator dies and, with probability b, a new predator is generated at the same location as the predator, with value of the perception range obtained from Eq (10).

For simplicity, we fix in this paper the values $r = d = c_0 = b = R_c = 1$ and focus our study in the influence of the different values of diffusion coefficients D_p and D_p, and mutation rate (for computational convenience we use also different values of system size L). The impact of changing the rates to other values is briefly addressed in section Summary and Discussion.

Mixing measures

In order to quantify the spatial arrangement of the species, we define measures of mixing. A possible way to proceed is to use the Shannon index or entropy, which has been applied to measure species diversity, racial, social or economic segregation on human population and as a clustering measure [33–35]. Based on these previous approaches, we propose a modification described below.

As usual, we start regularly partitioning the system in m square boxes with size $\delta x = L/\sqrt{m}$ and obtaining for each box i the *entropy index* s_i [34], given by

$$s_i = -f_p^{(i)} \ln f_p^{(i)} - f_v^{(i)} \ln f_v^{(i)} \,, \tag{12}$$

where $f_p^{(i)}$ ($f_v^{(i)}$) is the fraction of predators (preys) inside box i, i.e. $f_q^{(i)} = N_q^{(i)}/[N_p^{(i)} + N_v^{(i)}]$ with $q = p, n$ and $N_p^{(i)}$, $N_v^{(i)}$ the numbers of predators and preys in that box, respectively. In terms of Eq (12), predator-prey mixing is maximum when there is half of each type in the box, yielding $s_i = -\ln 1/2 = \ln 2$. Unbalancing the proportions of the two types in the box reduces s_i. If a box contains only predators or preys, $s_i = 0$, indicating perfect segregation. Finally, we define a whole-system predator-prey mixing measure by averaging the values s_i in the different boxes, each one weighted by its local population [34],

$$\langle\mathcal{M}\rangle_m \equiv \sum_{i=1}^{m} \frac{N^{(i)}}{N} s_i \,, \tag{13}$$

being $N^{(i)} = N_p^{(i)} + N_v^{(i)}$ the total box population and $N = N_v + N_p$ the total population. To really characterize the lack of inhomogeneity arising from interactions and mobility, one should compare the value of $\langle\mathcal{M}\rangle_m$ with the value $\overline{\mathcal{M}}$ that would be obtained by randomly locating the same numbers of predators and preys, N_p and N_v among the different boxes. At this point, approximations for $\overline{\mathcal{M}}$ which are only

appropriate if the number of individuals is large have been typically used. In our case, since predator and prey populations have large fluctuations, it is necessary to give a more precise estimation. In a brute force manner, one can obtain computationally the mixing measure for the random distribution simply by distributing randomly in the m spatial boxes the N_v preys and N_p predator and averaging the corresponding results of Eq (13) over many runs. On the other hand, this can be done analytically since we known that, for random spatial distribution, the number of individuals n_q of type q $(= p, v)$ in each box would obey a binomial distribution $B(n_q, N_q)$, where N_q is the total particle number in the system. We have that $B(n_q, N_q) = \binom{N_q}{n_q}(\frac{1}{m})^{n_q}(1 - \frac{1}{m})^{N_q - n_q}$. Then, Eq (13) for randomly mixed individuals becomes

$$\overline{\mathcal{M}} \equiv \sum_{n_v=0}^{N_v} \sum_{n_p=0}^{N_p} B(n_v, N_v) B(n_p, N_p) \frac{n_v + n_p}{N_v + N_p} s(n_v, n_p), \quad (14)$$

with s as defined in Eq (12).

Finally, a suitable measure of predator-prey mixing that characterizes spatial structure from the well-mixed case ($\mathcal{M} = 1$) to full segregation ($\mathcal{M} = 0$) is given by

$$\mathcal{M} \equiv \frac{\langle \mathcal{M} \rangle_m}{\overline{\mathcal{M}}}. \quad (15)$$

Also, we can define an analogous measure for each species' spatial distribution separately, which can be interpreted as a degree of clustering [35],

$$\mathcal{M}_v = -\frac{1}{\overline{\mathcal{M}}_v} \sum_i^m \frac{(N_v^{(i)}/N_v) \ln(N_v^{(i)}/N_v)}{m}, \quad (16)$$

and

$$\mathcal{M}_p = -\frac{1}{\overline{\mathcal{M}}_p} \sum_i^m \frac{(N_p^{(i)}/N_p) \ln(N_p^{(i)}/N_p)}{m}, \quad (17)$$

for preys and predators respectively, where

$$\overline{\mathcal{M}}_v = \sum_{n_v=0}^{N_v} B(n_v, N_v)[(n_v/N_v) \ln(n_v/N_v)], \quad \overline{\mathcal{M}}_p = \sum_{n_p=0}^{N_p} B(n_p, N_p)[(n_p/N_p) \ln(n_p/N_p)]. \quad (18)$$

For $\mathcal{M}_v$ or $\mathcal{M}_p = 1$, the corresponding species is well spread around the domain. Smaller values indicate clustering of the individuals.

The mixing measures are certainly affected by the size of the box δx used, which should be tuned to obtain maximum sensibility to the spatial distribution. For very large or very small box size, we see that different spatial distributions become indistinguishable. For instance, for the predator-prey mixing, if the box size is very large (of the order of system size), we will find that the predators and preys are well mixed independent on the values of the diffusion coefficients. On the other hand, if box size is very small it will be either occupied by a single predator or prey, if not empty, indicating segregation independently on the individuals mobility. In S4 Fig, we show how the mixing measure changes with box size δx and system size L for low mobility ($D_v = D_p = 0.1$), which produces a highly heterogeneous spatial distribution. We identify that for $\delta x \simeq 2$ maximum sensitivity with respect to diffusion coefficients is attained. We used $\delta x = 2$ in our results, being a suitable scale since it is also of the order of the typical values of the perceptual range attained under evolution. Regarding the system size, we found only weak variations in the mixing measures, which are shown in the inset of S4 Fig.

Supporting information

S1 Movie   Temporal evolution of population spatial distribution of predators and preys with low predator and prey mobilities. Predators and preys in colors red and blue, respectively, $D_p = D_v = 0.1$, mutation noise intensity $\sigma_\mu = 0.1$ and habitat size $L = 20$.

S2 Movie   Temporal evolution of population spatial distribution of predators and preys with high predator and prey mobilities. Predators and preys in colors red and blue, respectively, $D_p = D_v = 1$, mutation noise intensity $\sigma_\mu = 0.1$ and habitat size $L = 20$.

S1 Fig   Mixing measures as a function of predators perceptual range R in the non-evolving case. Predator-prey, prey and predator mixing for different values of diffusion coefficients as a function of predators' perceptual range R (which is fixed, not evolving, the same for all individuals and $\sigma_\mu = 0$). Vertical lines show the dominant perception range achieved through the evolutionary process under low mutation noise ($\sigma_\mu = 0.1$). $L = 10$.

S2 Fig   Normalized perceptual range probability density at long times and its temporal evolution. (A) $\bar{\rho}(R) = \rho(R)/N_p$ at long-times for low ($D_p = D_v = 0.1$) and high ($D_p = D_v = 1$) mobility. (B) $\bar{\rho}(R)$ at different times (initial condition is a sharp distribution at $R = 4$) obtained from the individual-level simulations for the high mobility case $D_n = D_p = 1$. In both panels habitat domain has size $L = 10$ and mutation intensity $\sigma_\mu = 0.1$. The perceptual range values are scaled by the optimal value $R_h^\star$ of the homogeneous case for comparison.

S3 Fig   Coexistence time probability distribution. Coexistence time probability distribution obtained from individual-level simulations with $D_v = D_p = 1, 10, 100$, mutation intensity $\sigma_\mu = 1.0$ and habitat size $L = 10$. Inset shows the behavior at short timescale for the same cases. Solid red lines indicate an exponential distribution with the same mean.

S4 Fig   Mixing measures as a function of the box size used in their calculation, and of system size. Average mixing measures for the low mobility case $D_p = D_v = 0.1$ for different box sizes δx. Mutation intensity $\sigma_\mu = 0.1$ and habitat size $L = 10$. Inset shows the dependence on system size L for $\delta x = 2$ (for systems sizes in which it is not possible to set this value we take the closest points). Averages are performed over time and realizations in the long-time regime.

Acknowledgments

References

1. Azaele S, Suweis S, Grilli J, Volkov I, Banavar JR, Maritan A. Statistical mechanics of ecological systems: Neutral theory and beyond. Rev Mod Phys. 2016;88:035003. doi:10.1103/RevModPhys.88.035003.

2. Ayala FJ. Competition between species: frequency dependence. Science. 1971;171(3973):820–824.

3. Chesson P. Mechanisms of Maintenance of Species Diversity. Annual Review of Ecology and Systematics. 2000;31(1):343–366. doi:10.1146/annurev.ecolsys.31.1.343.

4. Tarnita CE, Washburne A, Martínez-García R, Sgro AE, Levin SA. Fitness tradeoffs between spores and nonaggregating cells can explain the coexistence of diverse genotypes in cellular slime molds. Proceedings of the National Academy of Sciences. 2015;112(9):2776–2781. doi:10.1073/pnas.1424242112.

5. Martínez-García R, Tarnita CE. Seasonality can induce coexistence of multiple bet-hedging strategies in Dictyostelium discoideum via storage effect. Journal of Theoretical Biology. 2017;426:104–116.

6. Tilman D. Competition and biodiversity in spatially structured habitats. Ecology. 1994;75(1):2–16.

7. Amarasekare P. Competitive coexistence in spatially structured environments: a synthesis. Ecology Letters. 2003;6(12):1109–1122.

8. Siepielski AM, Nemirov A, Cattivera M, Nickerson A. Experimental Evidence for an Eco-Evolutionary Coupling between Local Adaptation and Intraspecific Competition. The American Naturalist. 2016;187(4):447–456. doi:10.1086/685295.

9. Kotil SE, Vetsigian K. Emergence of evolutionarily stable communities through eco-evolutionary tunnelling. Nature Ecology and Evolution. 2018;2(10):1644–1653. doi:10.1038/s41559-018-0655-7.

10. Hiltunen T, Ayan GB, Becks L, Ayan B, Becks L. Environmental fluctuations restrict eco-evolutionary dynamics in predator – prey system. Proceedings of the Royal Society B. 2015;282:20150013. doi:10.1098/rspb.2015.0013.

11. Saccheri I, Hanski I. Natural selection and population dynamics. Trends in Ecology & Evolution. 2006;21(6):341–347. doi:10.1016/j.tree.2006.03.018.

12. Pelletier F, Garant D, Hendry AP. Eco-evolutionary dynamics. Philosophical Transactions of the Royal Society B: Biological Sciences. 2009;364(1523):1483–1489. doi:10.1098/rstb.2009.0027.

13. Govaert L, Fronhofer EA, Lion S, Eizaguirre C, Bonte D, Egas M, et al. Eco-evolutionary feedbacks - theoretical models and perspectives. Functional Ecology. 2018;(October):1–18. doi:10.1111/1365-2435.13241.

14. Yoshida T, Jones LE, Ellner SP, Fussmann GF, Hairston Jr NG. Rapid evolution drives ecological dynamics in a predator–prey system. Nature. 2003;424:303–306. doi:10.1038/nature01767.

15. Yamamichi M, Yoshida T, Sasaki A. Comparing the effects of rapid evolution and phenotypic plasticity on predator-prey dynamics. The American Naturalist. 2011;178(3):287–304.

16. Bonachela JA, Wortel MT, Stenseth NC. Eco-evolutionary Red Queen dynamics regulate biodiversity in a metabolite-driven microbial system. Scientific Reports. 2017;7(1):1–9. doi:10.1038/s41598-017-17774-4.

17. Bohannan BJ, Lenski RE. Effect of prey heterogeneity on the response of a model food chain to resource enrichment. The American Naturalist. 1999;153(1):73–82.

18. Becks L, Ellner SP, Jones LE, Hairston Nelson G JG. Reduction of adaptive genetic diversity radically alters eco-evolutionary community dynamics. Ecology Letters. 2010;13(8):989–997. doi:10.1111/j.1461-0248.2010.01490.x.

19. Cortez MH, Weitz JS. Coevolution can reverse predator-prey cycles. Proceedings of the National Academy of Sciences. 2014;111(20):7486–7491. doi:10.1073/pnas.1317693111.

20. Abrams PA. The Evolution of Predator-Prey Interactions: Theory and Evidence. Annual Review of Ecology and Systematics. 2001;31(12):79–105. doi:10.1146/annurev.ecolsys.31.1.79.

21. Cortez MH, Ellner SP. Understanding rapid evolution in predator-prey interactions using the theory of fast-slow dynamical systems. The American Naturalist. 2010;176(5):329–341. doi:10.1086/687393.

22. Hanski I, Mononen T. Eco-evolutionary dynamics of dispersal in spatially heterogeneous environments. Ecology Letters. 2011;14(10):1025–1034. doi:10.1111/j.1461-0248.2011.01671.x.

23. Fronhofer EA, Altermatt F. Classical metapopulation dynamics and eco-evolutionary feedbacks in dendritic networks. Ecography. 2017;40(12):1455–1466. doi:10.1111/oik.03652.

24. Zollner PA. Comparing the landscape level perceptual abilities of forest sciurids in fragmented agricultural landscapes. Landscape Ecology. 2000;15(6):523–533.

25. Fagan WF, Gurarie E, Bewick S, Howard A, Cantrell RS, Cosner C. Perceptual Ranges, Information Gathering, and Foraging Success in Dynamic Landscapes. The American Naturalist. 2017;189(5):474–489. doi:10.1086/691099.

26. Martínez-García R, Calabrese JM, Mueller T, Olson KA, López C. Optimizing the search for resources by sharing information: Mongolian gazelles as a case study. Physical Review Letters. 2013;110(24). doi:10.1103/PhysRevLett.110.248106.

27. Martínez-García R, Calabrese JM, López C. Optimal search in interacting populations: Gaussian jumps versus Lévy flights. Physical Review E. 2014;89(3). doi:10.1103/PhysRevE.89.032718.

28. Lingle S. Anti-predator strategies and grouping patterns in white-tailed deer and mule deer. Ethology. 2001;107(4):295–314.

29. Vulinec K. Collective security: aggregation by insects as a defense. Insect defenses. 1990; p. 251–288.

30. Young WR, Roberts AJ, Stuhne G. Reproductive pair correlations and the clustering of organisms. Nature. 2001;412(6844):328–31. doi:10.1038/35085561.

31. Martínez-García R, Calabrese JM, López C. Online games: a novel approach to explore how partial information influences human random searches. Scientific Reports. 2017;7:40029.

32. Bird A. Perceptions of epigenetics. Nature. 2007;447:396.

33. Jost L. Entropy and diversity. Oikos. 2006;113(2):363–375.

34. White MJ. Segregation and Diversity Measures in Population Distribution. Population Index. 1986;52(2):198–221.

35. López C. Self-propelled nonlinearly diffusing particles: Aggregation and continuum description. Phys Rev E. 2005;72:061109. doi:10.1103/PhysRevE.72.061109.

36. Rossine FW, Martinez-Garcia R, Sgro AE, Gregor T, Tarnita CE. Eco-evolutionary significance of 'loners'. bioRxiv. 2018; p. 508507.

37. Hastings A, Harrison S. Metapopulation dynamics and genetics. Annual Review of Ecology and Systematics. 1994;25(1):167–188.

38. Whittaker RH. Evolution and Measurement of Species Diversity. Taxon. 1972;21(2/3):213–251. doi:10.2307/1218190.

39. Socolar JB, Gilroy JJ, Kunin WE, Edwards DP. How Should Beta-Diversity Inform Biodiversity Conservation? Trends in Ecology & Evolution. 2016;31(1):67 – 80. doi:https://doi.org/10.1016/j.tree.2015.11.005.

40. ter Hofstede HM, Ratcliffe JM. Evolutionary escalation: the bat–moth arms race. Journal of Experimental Biology. 2016;219(11):1589–1602. doi:10.1242/jeb.086686.

41. Heinsalu E, Hernández-García E, López C. Spatial clustering of interacting bugs: Lévy flights versus Gaussian jumps. EPL (Europhysics Letters). 2010;92(4):40011. doi:10.1209/0295-5075/92/40011.

42. Pigolotti S, Benzi R, Jensen MH, Nelson DR. Population Genetics in Compressible Flows. Phys Rev Lett. 2012;108:128102. doi:10.1103/PhysRevLett.108.128102.

43. MacKenzie BR, Miller TJ, Cyr S, Leggett WC. Evidence for a dome-shaped relationship between turbulence and larval fish ingestion rates. Limnology and Oceanography;39(8):1790–1799. doi:10.4319/lo.1994.39.8.1790.

44. Gillespie DT. Exact stochastic simulation of coupled chemical reactions. The Journal of Physical Chemistry. 1977;81(25):2340–2361. doi:10.1021/j100540a008.

45. Birch DA, Young WR. A master equation for a spatial population model with pair interactions. Theoretical Population Biology. 2006;70(1):26 – 42. doi:https://doi.org/10.1016/j.tpb.2005.11.007.

46. Heinsalu E, Hernández-García E, López C. Competitive Brownian and Lévy walkers. Phys Rev E. 2012;85:041105. doi:10.1103/PhysRevE.85.041105.